

理學碩士 學位論文

# Hydrothermal growth and characterization of indium doped ZnO nanorod



指導教授 金泓承

2013 年 8 月

韓國海洋大學校 大學院

應用科學科 半導體物理專攻

張 帆

本 論 文 을 張 帆 의  
理 學 碩 士 學 位 論 文 으 로 認 准 함 .

委 員 長 梁 璿 (印)

委 員 金 泓 承 (印)

委 員 張 樂 元 (印)



2013 年 8 月

韓 國 海 洋 大 學 校 大 學 院

# Content

<b>List of Tables</b> .....	III
<b>List of Figures</b> .....	IV
<b>Abstract</b> .....	V
<b>Chapter 1. Introduction</b> .....	1
<b>Chapter 2. Basic properties of ZnO</b> .....	3
2.1 Research underground of ZnO.....	3
2.2 The growth of ZnO.....	6
2.2.1 Deposition of ZnO seed layer (RF-Sputter).....	6
2.2.1.1 Introduction of RF-sputter.....	6
2.2.1.2 ZnO deposition.....	8
2.2.2 Hydrothermally method.....	10
2.2.2.1 Introduction of hydrothermal system.....	10
2.2.2.2 Growth mechanism of hydrothermal method.....	10
2.2.2.3 The growth of In-doped ZnO nanorod.....	12
2.3 Characterization methods of doped ZnO nanostructure.....	13
2.3.1 X-Ray Diffraction.....	13
2.3.2 Scanning Electronic Microscopy (SEM).....	16
2.3.3 X-ray Photoelectron Spectroscopy (XPS).....	18

2.3.4 Photoluminescence (PL) Spectrum.....	20
<b>Chapter 3. In doped ZnO nanorod .....</b>	<b>22</b>
3.1 Experimental detail.....	22
3.2 Results and discussions.....	23
3.2.1 Characterization of In-doped ZnO nanorod .....	23
3.2.2 The growth mechanism of ZnO affected by indium impurity .....	36
<b>Chapter 4. In-doped ZnO nanostructure .....</b>	<b>38</b>
4.1 Experimental detail.....	38
4.2 Results and discussions.....	39
<b>Chapter 5. Conclusion.....</b>	<b>40</b>
<b>References .....</b>	<b>42</b>



## List of Tables

<b>Table 1</b> The basic properties of zinc oxide .....	4
<b>Table 2</b> The detail growth condition of un-doped zno and In doped ZnO with various indium concentration .....	22
<b>Table 3</b> Atomic concentration of undoped ZnO and indium doped ZnO nanorods.....	32
<b>Table 4</b> The area ratio of different peak fitted into o 1s peak of different samples .....	32
<b>Table 5</b> The detail growth condition of un-doped ZnO and In doped ZnO with various indium concentration .....	38



## List of Figures

<b>Fig. 1</b> Schematic drawing of various types of chemical bonding of solids and their electronic properties. ....	3
<b>Fig. 2</b> The wurtzite hexagonal structure of ZnO .....	5
<b>Fig. 3</b> Systematic structure of magnetron RF-sputter.....	7
<b>Fig. 4</b> Drawing of deposition process.....	8
<b>Fig. 5</b> Schematic of the reactor system used for the growth of ZnO nanorods on various substrates. ....	10
<b>Fig. 6</b> Schematic diagrams for the growth of In-doped ZnO nanorod .....	12
<b>Fig. 7</b> X-ray diffraction diagram .....	14
<b>Fig. 8</b> The principle of XRD system .....	15
<b>Fig. 9</b> Schematic describing the operation of an SEM.....	17
<b>Fig. 10</b> The drawing of photoelectric effect .....	19
<b>Fig. 11</b> Various recombination processes in semiconductor (a) inter-band transition, (b) band-impurity center radiation recombination, (c) donor-acceptor radiation recombination	21
<b>Fig. 12</b> The In content (EDAX) value of In-doped ZnO nanorod with different In source varied from 5 to 50 wt.% .....	23
<b>Fig. 13</b> The XRD patterns of In-doped nanorod with various In source .....	25
<b>Fig. 14</b> SEM images of In-doped ZnO nanorod: (a) pure ZnO nanorod, (b) indium source: 5 wt.%, (c) indium source: 10 wt.%, (d) indium source: 25 w.%, (e) indium source: 50 wt.%.....	27
<b>Fig. 15</b> Diameters and length of pure ZnO and In-doped ZnO nanorods with different In source varied from 5 to 50 wt.%.....	28
<b>Fig. 16</b> XPS spectrum: (a) full range, (b) Zn 2p <sup>3/2</sup> , (c) In 3d <sup>5/2</sup> , and (d) O 1s.....	31
<b>Fig. 17</b> RT-PL patterns of pure ZnO and In-doped ZnO nanorod with different In source varied from 5 to 50 wt.% .....	34
<b>Fig. 18</b> The intensity ratio of UV emission to visible emission of pure ZnO and In-doped ZnO nanorods .....	35
<b>Fig. 19</b> SEM images of In-doped ZnO nanorod with In content at 10 wt.%.....	39

# Hydrothermal growth and characterization of indium doped ZnO nanorod

Fan Zhang

*Major in Semiconductor Physics  
Department of Applied Science  
Graduate School of Korea Maritime University*

## Abstract

In recent decades, ZnO nanorod was widely used nanostructure for applications such as ZnO based light emitting diodes, field-effect transistor and laser diodes owing to its electrical, structural and optical properties, which depend strongly on the size, defect concentration, along with surface characteristics. To realize the purpose of changing the morphology and improving the opt electrical properties, indium doped ZnO nanorods were grown on ZnO seed layer by hydrothermal method. In this study, the growth and the relationship of the morphology and indium concentration of In-doped ZnO nanorods were theoretically demonstrated.

In the chapter 1, introduction about this study was briefly described. The basic properties, growth process (especially growth mechanism of hydrothermal method), characterization of In-doped ZnO nanorod were introduced in chapter 2 and 3. The chapter 4 reveals the effects of In content on the In-doped ZnO nanorods. The structural and optical properties were investigated by X-ray spectroscopy, field emission scanning electron microscopy and photoluminescence. In chapter 5, the different In-doped ZnO

nanostructure was grown by using different Indium material and the growth mechanism of that nanostructure was discussed at detail. Finally, results were summarized and concluded.

**KEY WORDS:** ZnO, Indium, nanorod, hydrothermal method





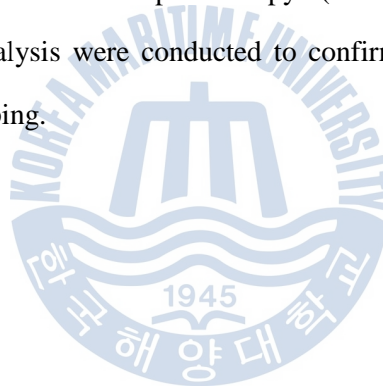
## Chapter 1. Introduction

Recently, ZnO has attracted large attention as a promising material due to its good opt-electrical, piezoelectric properties and excellent chemical, thermal stability. Besides that, it is II-VI semiconductor with wide band gap (3.37eV) and high exciton binding energy (60meV). Thus, it is widely used in a broad range of technological applications such as ultraviolet laser, transparent conducting oxide electrode, solar cell, field-effect transistor and sensors. Among its nanostructure form, one dimensional nanorod has advantages over others because of its excellent optical transmission properties [1], highly orientation [2], and high specific surface ratio [3].

However, the resistance of pure ZnO is high resulting from the low carrier, which leads the devices made of pure ZnO has low sensitivity, low stability and slow response rate. By controlling the growth, doping and assembling of ZnO, we can improve the electrical, optical, and magnetic properties, in order to better applied to UV laser transmitter, high efficient transparent equipment, surface acoustic wave device, piezoelectric transducer, and sensors [4-8]. It has been observed that the group III elements, such as Al, Ga, and In, was widely used as n-type dopants to fabricate n-type ZnO with good quality and low resistivity, as they can substitute Zn ions and occupy the Zn vacancies. Hence, several approaches have been proposed for the growth of 1-D ZnO nanostructures with various doping elements via hydrothermally method and thermal evaporation method. For example, Junjie Qi et al. grew In-doped nanodisk by In doping [9]. A. Escobedo-Morales et al. discussed the defect annihilation and morphological of hydrothermally grown ZnO nanorods by Ga doping [10]. Compared to other element doping, such as Ga, Al, In doping has obvious advantages over others. By indium doping, we could get ZnO with high electronic conductivity, unique thermal stability, good chemical stability and excellent optical properties. Jie et al. made In doped ZnO nanowire

and nano-flower shaped ZnO by thermal evaporation method [11]. Systematic research on In doped ZnO nanorod was lacked and thus, we did research on it. Additionally, hydrothermal method had advantages of large scale product yield and sample uniformity at a relatively low temperature.

In this research, we grew ZnO nanorod with In dopants under different concentration on Si substrates with ZnO buffer layer by hydrothermally method successfully. The structural properties were investigated by field emission scanning electron microscope (FESEM). The Energy Dispersive Spectrometer was carried out using an EDAX system equipped with a high-resolution SEM. The chemical composition of the samples was determined by X-ray photoelectron spectroscopy (XPS). The Room temperature photoluminescence (PL) analysis were conducted to confirm that the optical properties could be improved by In doping.



## Chapter 2. Basic properties of ZnO

### 2.1 Research underground of ZnO

As a candidate material for optoelectronic devices, ZnO has a relatively high exciton binding energy ( $\sim 60\text{meV}$ ) and shows an intense ultraviolet emission for lasing at room temperature due to its wide band gap ( $\sim 3.37\text{eV}$ ). Figure 1 Shown the schematic drawing of various types of chemical bonding of solids and their electronic properties. As we can see, ZnO already has a substantial ionic bonding component, which shows ZnO in the centre of “centre of solid state physics” [12]. Specific properties of ZnO are listed in Table 1. These properties make it appropriate as a new kind of wide bandgap semiconductor in different nanostructure from, such as thin films, nanodisk, nanowire, flower-like nanostructure and nanorod etc. therefore, more and more attention has been paid to ZnO using in light emitting diodes (LED), transparent conductive diode, surface acoustic devices and solar cells.

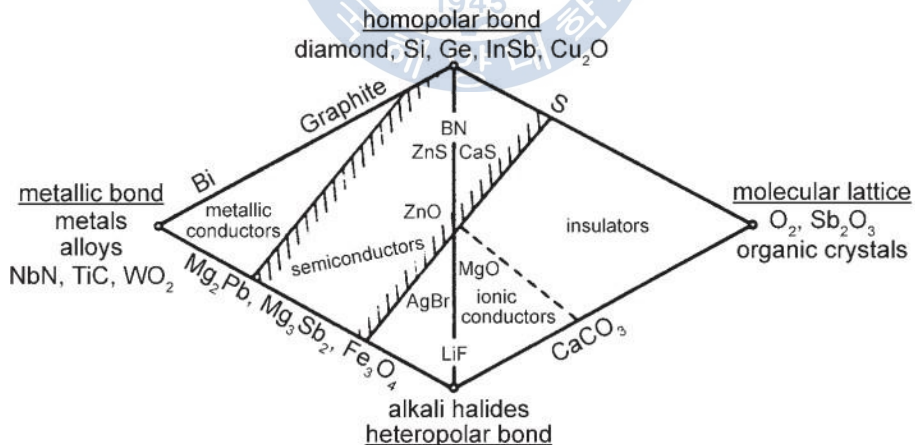


**Fig. 1** Schematic drawing of various types of chemical bonding of solids and their electronic properties.

**Table 1** The basic properties of zinc oxide

Properties	Value
Molecular weight	81.389
Density (g/cm <sup>3</sup> )	5.642
Melting point (°C)	1975
Special heat (cal/g*m)	0.125
Thermoelectric constant (m*V/K)	1200(at 300K)
Electric conductivity (Ω*cm)	10
Linear thermal-expansion coefficient (K <sup>-1</sup> )	4.25 (a-axis), 2.92 (c-axis)
Mott hardness	4.5
Thermal conductivity (W/cm*K)	1.16±0.08 (Zn face), 1.10±0.09 (O face)
Shear modulus (GPa)	~45
Band gap (RT)	3.37eV
Electric binding energy (meV)	60
Radiation resistance	2MeV, 1.2×10 <sup>17</sup> electronics/cm

Besides that, ZnO crystallizes in the hexagonal wurtzite-type structure naturally shown in Figure 2. It has a polar hexagonal axis, the c-axis, which is parallel to z. Its point group is  $C_{6v}$ , and the space group is  $P6_3mc$ . One zinc ion is surrounded tetrahedral by four oxygen ions and vice versa. According to X-ray data 36-1451 published by Joint Committee on Power Diffraction Standards (JCPDS), the lattice constants of ZnO are 0.5206 nm along c-axis and 0.3249 nm along a-axis. Unlike other II-VI semiconductor, which exist both in the cubic zinc blende and the hexagonal wurtzite structures, ZnO crystallizes with great preference in the wurtzite-type structure.

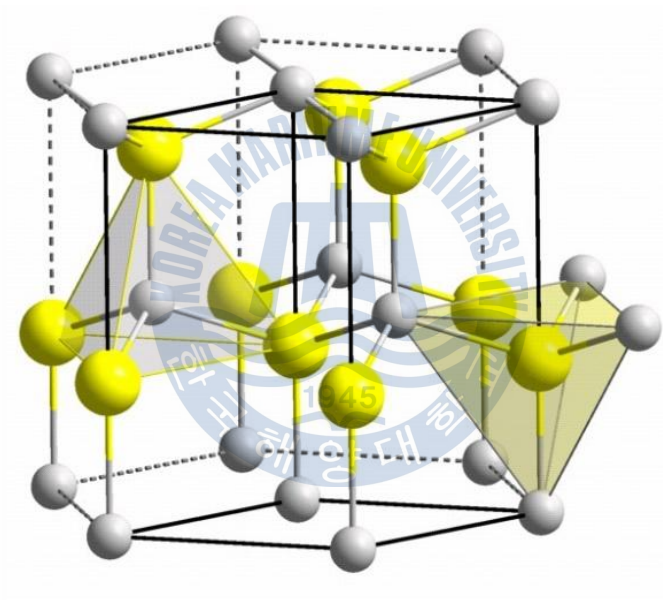


**Fig. 2** The wurtzite hexagonal structure of ZnO

## **2.2 The growth of ZnO**

Nowadays, the growth method of ZnO could be divided into physical and chemical methods according to the synthesis of nano-ZnO. Physical method refers prepare nano-ZnO based devices using thin film' growth and nanolithography which needs discrete and expensive system and remains many difficulties to overcome. Otherwise, the chemical growth means that from the atoms or nucleation of molecules, grow or condenses into small particles with certain size and shape. It contains three kinds of methods: solid phase method, liquid phase method, and vapor phase method. Among them, liquid and vapor phase method have a variety of ways, such as Chemical Vapor Deposition (CVD), Molecular-Beam Epitaxy (MBE), Metal Organic Chemical Vapor Deposition (MOCVD), Radio-Frequency Magnetron Sputtering (RFMS), Metal Organic Vapor Phase Epitaxy (MOVPE), Thermal Pyrolysis and Sol-gel method, Hydrothermal method etc. Nanometer-ZnO is mainly prepared by liquid and vapor phase method in experiment. We assumed PRMS and Hydrothermal method to prepare ZnO seed layer and ZnO nanarod respectively, which will be discussed at detail in the next chapter.

### **2.2.1 Deposition of ZnO seed layer (RF-Sputter)**

#### **2.2.1.1 Introduction of RF-sputter**

Sputter deposition is a physical vapor deposition process for depositing thin films, which means ejecting material from a target and depositing it on a substrate such as a silicon wafer. The target is the source material. Substrates are placed in a vacuum chamber and are pumped down to a prescribed process pressure. Sputtering starts when a negative charge is applied to the target material causing a plasma region or glow discharge. Positive charged gas ions generated in the plasma region are attracted to the negatively biased target plate at a very high speed. This collision creates a momentum transfer and

ejects atomic size particles from target. These particles are deposited as a thin film into the surface of substrates.

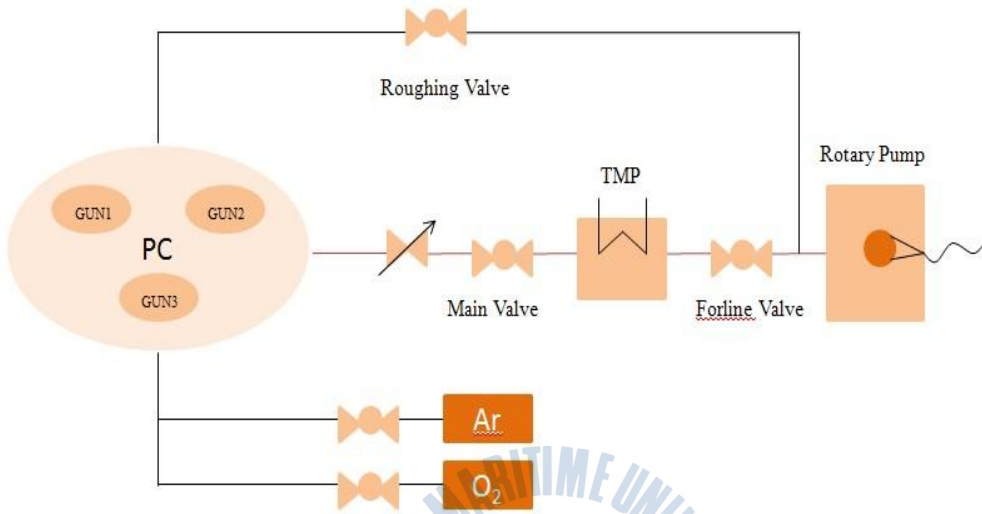


**Fig. 3** Systematic structure of magnetron RF-sputter

Analva-SPF-322H sputtering system, shown in Fig.3 is equipped with three 3-inch diameter planar magnetron cathodes to facilitate multi layers with target shutter and pre-sputtering shutter and with a rotatable substrate holder shown in Fig.4. The targets consists of three kinds: ZnO, MgO, and MgZnO and also the substrates can be heated up to 300°C to improve the films applied to various condition for experiment. The Argon and Oxygen gas can be induced to the vacuum chamber for the ultimate pressure reached to approximately  $4 \times 10^{-6}$  Pa.

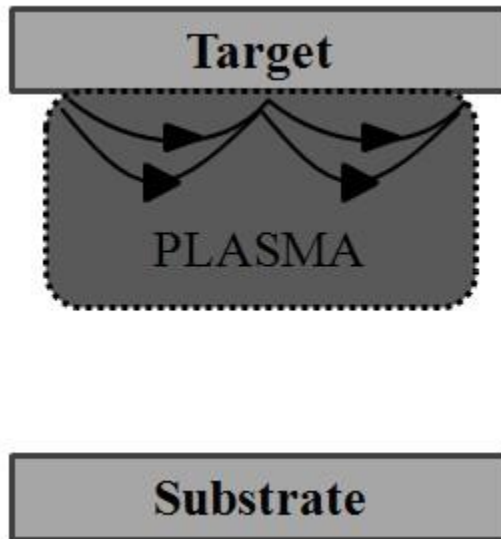


**Fig. 4** Drawing of deposition process

Magnetron sputtering can be done either DC or RF modes. DC sputtering is done with conducting material. If the target is non conducting material the positive charge will build up on the material and it will stop sputtering. RF sputtering can be done both conducting and non conducting materials. Here, magnets are used to increase the percentage of electrons that take part in ionization of events and thereby increase the probability of electrons striking the Argon atoms, increase the length of the electron path, and hence increase the ionization efficiency significantly.

#### **2.2.1.2 ZnO deposition**

The ZnO seed layer was grown on the silicon (Si) substrate which firstly cleaned in acetone, methanol, and then deionized (DI) water for 5 minutes respectively. Besides that, the silicon substrate was ultimately cleaned by HF to move the oxide phase.

After that, the sputter system is started. Prior to deposition, the chamber was vacuumed to  $2 \times 10^{-6}$  Torr. Ar gas was introduced through mass flow controllers (MFC) at a rate of 20 sccm. ZnO was used as the target and the RF power was increased to 100W to



create plasma. Before deposition, it was pre-sputtered for 10 minutes. During the deposition, the chamber pressure was maintained at 5 mTorr at room temperature and the deposition time was kept as 30 minutes. After deposition, the thickness of ZnO seed layer was approximately 100 nm.



## 2.2.2 Hydrothermally method

### 2.2.2.1 Introduction of hydrothermal system

The ZnO nanorod was grown successfully in the hydrothermal system. It consists of temperature sensor, hot plate, round bottom flask, substrate holder and Si oil as shown in figure 5. As we can see, the holder could be used for substrates with various materials, shape, and size. The spin bar in the Si oil rotated to heat evenly and the Si oil is applied to create a homogenous temperature surround the round bottom flask. The reaction temperature could be varied from 60°C to 400°C by temperature sensor whereas the growth temperature was kept as constant at 95°C for In-doped ZnO nanorod.

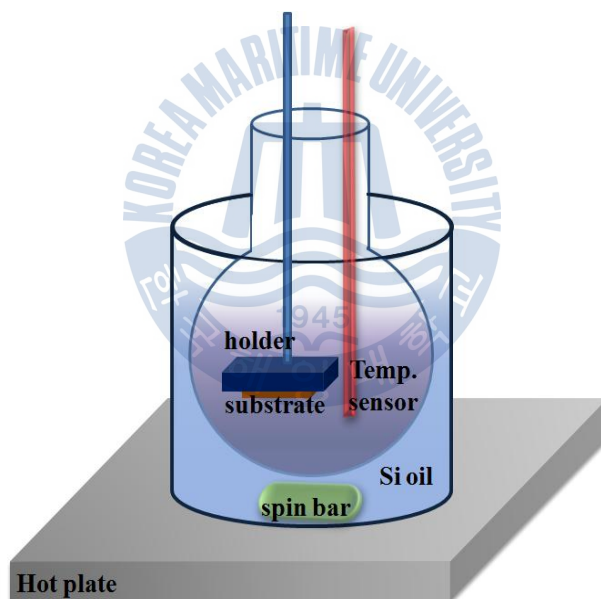
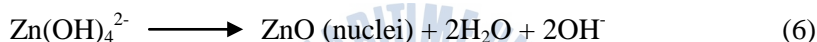
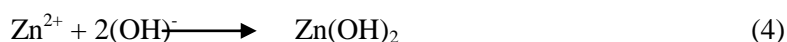
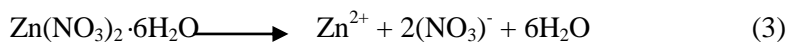
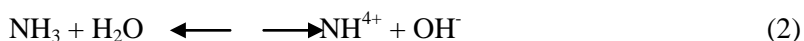


**Fig. 5** Schematic of the reactor system used for the growth of ZnO nanorods on various substrates.

### 2.2.2.2 Growth mechanism of hydrothermal method

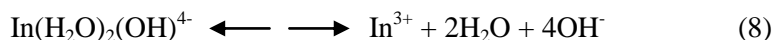
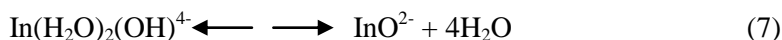
The hydrothermal method, as an aqueous solution method, is processed by chemical reactions in a reaction solution. The zinc nitrate hexahydrate ( $\text{Zn}(\text{NO}_3)_2 \cdot 6\text{H}_2\text{O}$ , Kanto Chemical, purity 99.0 %) and hexamethylenetetramine (HMT, Kanto Chemical, purity

99.0 %) were mixed together with dopant materials such as Indium acetate hydrate ( $\text{In}(\text{CH}_3\text{CO}_2)_3 \cdot x\text{H}_2\text{O}$ ), and Indium chloride ( $\text{In}_2\text{Cl}_3$ ) in a reaction solution with DI water, yielding the following reactions:



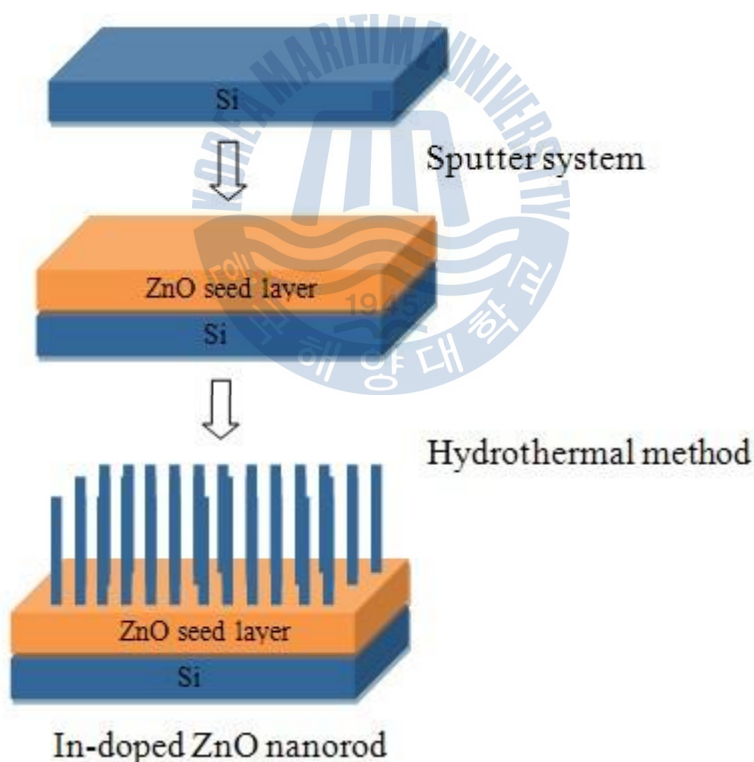
The  $\text{Zn}(\text{OH})_2$  dissolves in the solution to form growth units, which are negatively charged complexes, the simplest one of which is  $\text{Zn}(\text{OH})_4^{2-}$ , an anionic coordination tetrahedron.

However, the growth mechanism of ZnO in the presence of dopant, as well as Ga, In, etc. is slightly changed. Once the dopant (such as Ga, In) is introduced into the solution, we assumed that  $\text{In}(\text{H}_2\text{O})_2(\text{OH})_4^{4-}$  would produce octahedral growth units which could be incorporated into the ZnO crystal and then the dopant (such as In, Ga, etc.) would replace the zinc sites on some extent. Addition, the growth mechanism of indium doped ZnO nanorod will be discussed detail in the later.



### 2.2.2.3 The growth of In-doped ZnO nanorod

The schematic diagrams for the growth of In-doped ZnO nanorod using by hydrothermal process on various substrates was shown in figure 6. A certain amount of zinc nitrate hexahydrate ( $\text{Zn}(\text{NO}_3)_2 \cdot 6\text{H}_2\text{O}$ ) and the same amount of hexamethylenetetramine (HMT) were dissolved into 100ml DI water respectively and heated, then mixed together in the round bottom flake. After that, different quantitative dopant material was added into the mixed solution which is immersed into the Si oil. The reaction temperature is  $95^\circ\text{C}$  and the growth time is 1 hour.

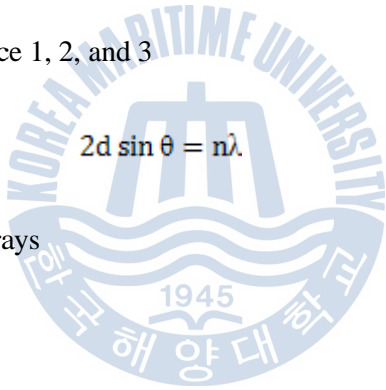


**Fig. 6** Schematic diagrams for the growth of In-doped ZnO nanorod

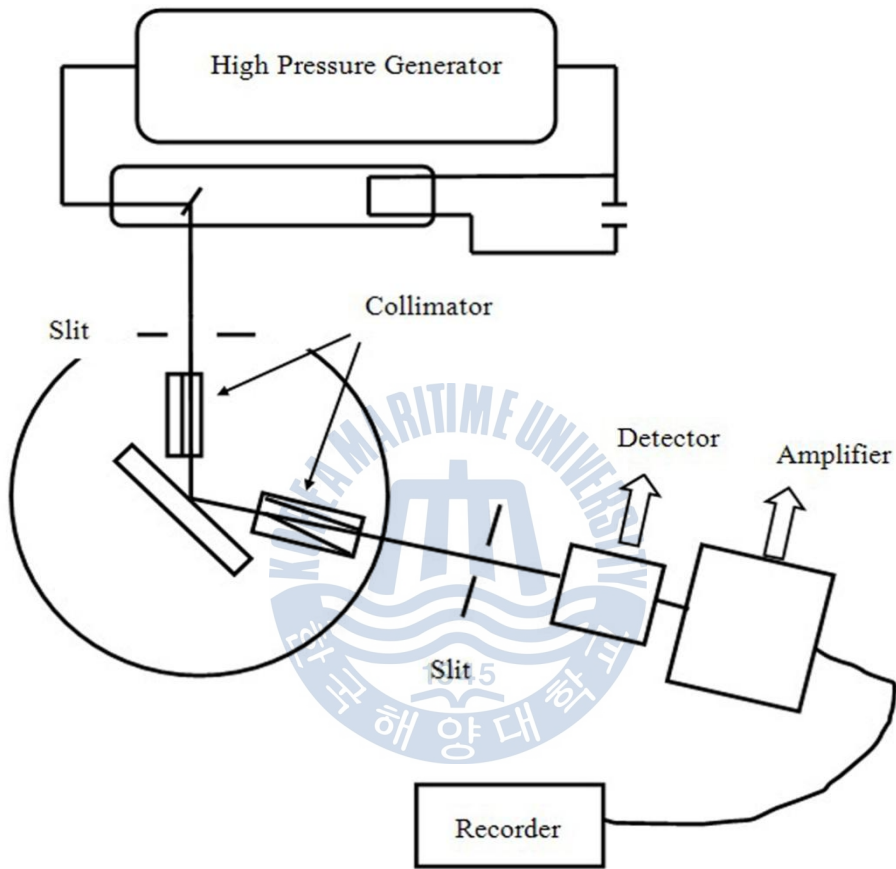
## 2.3 Characterization methods of doped ZnO nanostructure

### 2.3.1 X-Ray Diffraction

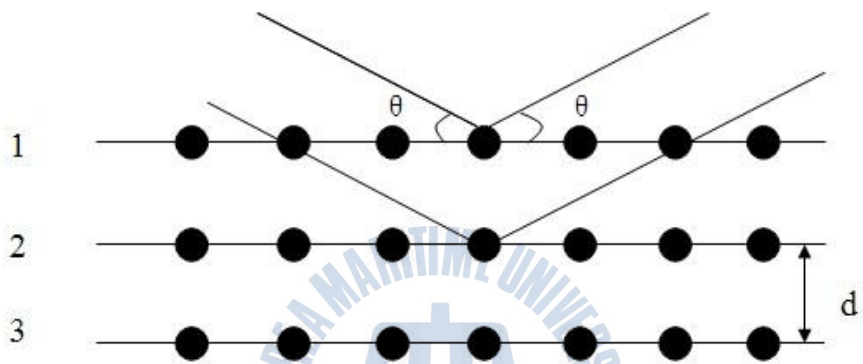
X-ray diffraction (figure 7) is widely used in measuring the crystal structure as an important analysis method. X-rays have wavelengths on the order of a few angstroms (1 Angstrom = 0.1 nm). This is the typical inter-atomic distance in crystalline solid; making X-rays the correct order of magnitude for diffraction of atoms of crystalline materials. When X-rays are scattered from a crystalline solid they can constructively interfere, producing a diffracted beam. The relationship describing the angle at which a beam of X-rays of a particular wavelength diffracts from a crystalline surface was discovered by Sir William H. Bragg and Sir W. Lawrence and is known as Bragg's Law. As it is shown in figure 8, the planar interface 1, 2, and 3


$$2d \sin \theta = n\lambda$$

- $\lambda$  wavelength of x-rays
- $\theta$  scattering angle
- $d$  inter-plane distance of (i.e atoms, ions, molecules)
- integer representing the order of the diffraction peak



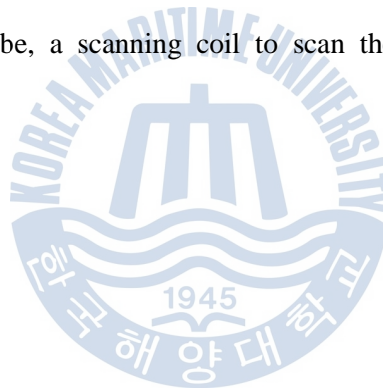
**Fig. 7** X-ray diffraction diagram



**Fig. 8** The principle of XRD system

### 2.3.2 Scanning Electronic Microscopy (SEM)

The Scanning Electron Microscope (SEM) is used for observations of specimen surfaces. When the specimen is irradiated with a fine electron beam (called an electron probe), secondary electrons are emitted from the specimen surface. Topography of the surface can be observed by two-dimensional scanning of the electron probe over the surface and acquisition of an image from the detected secondary electrons. The SEM requires an electron optical system to produce an electron probe, a specimen stage to place the specimen, a secondary-electron detector to collect secondary electrons, an image display unit, and an operation system to perform various operations (figure 9). The electron optical system consists of an electron gun, a condenser lens and an objective lens to produce an electron probe, a scanning coil to scan the electron probe, and other components.





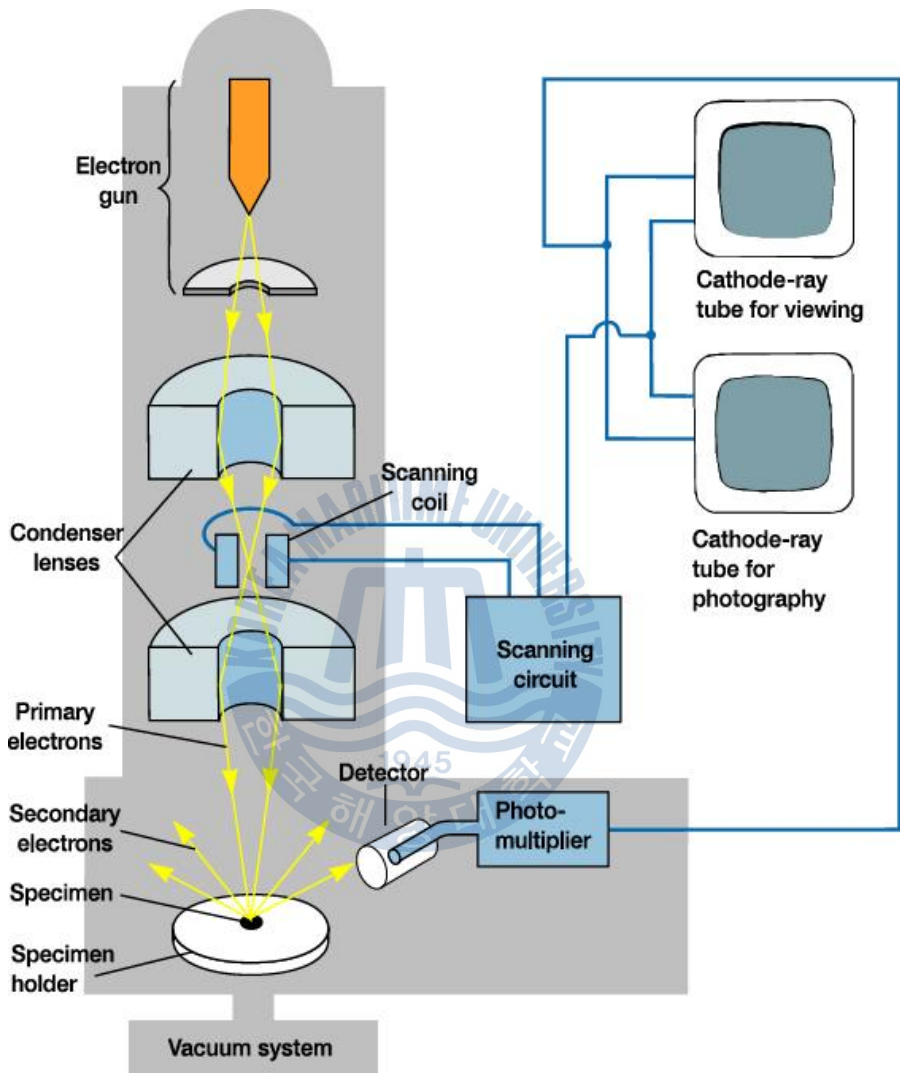


**Fig. 9** Schematic describing the operation of an SEM.

### 2.3.3 X-ray Photoelectron Spectroscopy (XPS)

X-ray Photoelectron Spectroscopy (XPS), also known as Electron Spectroscopy for Chemical Analysis (ESCA) is a widely used technique to investigate the chemical composition of surfaces. As shown in figure 10, XPS makes use of the photoelectric effect. When the material is exposure to the incident X-ray, the atom of the material will release ejected photo electron as following the process:

$$E_{\text{Binding}} = E_{\text{Photon}} - (E_{\text{kinetic}} + \Phi)$$

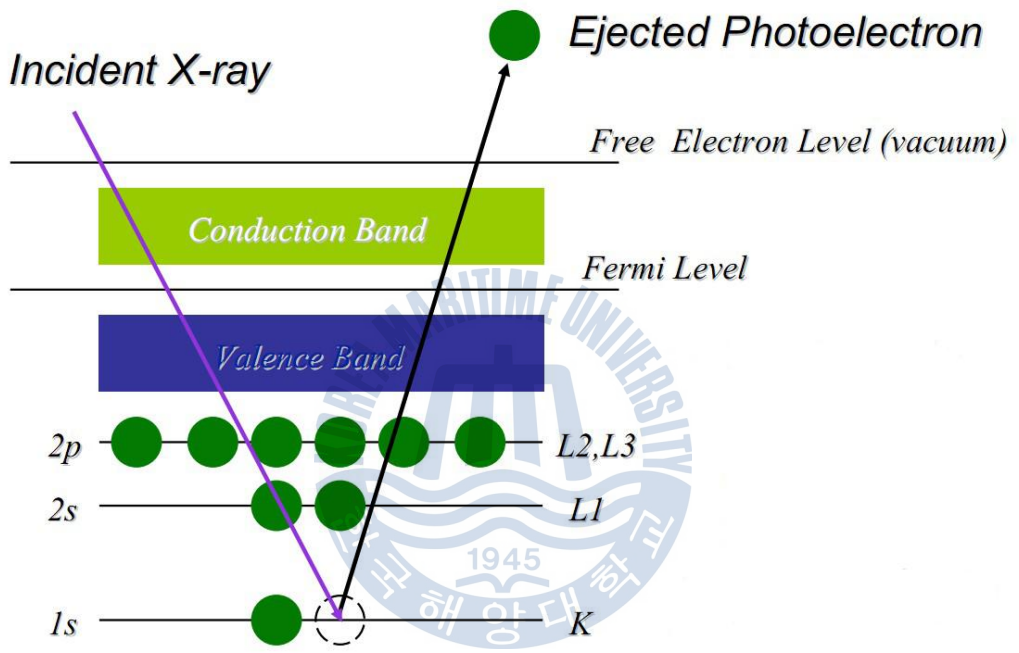
$E_{\text{Binding}}$  ---- the binding energy of the electron

$E_{\text{Photon}}$  ---- the energy of the X-ray photons being used

$E_{\text{kinetic}}$  ---- the kinetic energy of the electron as measured by the instrument

$\Phi$  ---- the work function of the spectrometer

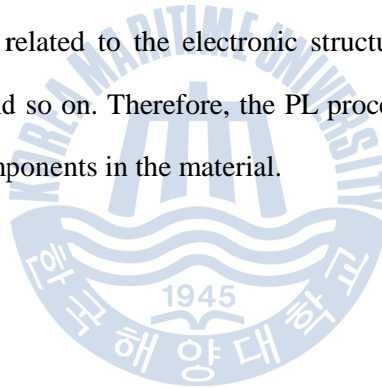
As we known, each atom produces a characteristic set of XPS peaks at characteristic binding energy values that directly identify each element exist in or on the surface of the material being analyzed. These unique peaks correspond to the electron configuration of the electrons within the atoms, e g., 1s, 2p, 3s etc. And the number of detected electrons in each of the unique peaks is directly related to the amount of the element within the area irradiated.



**Fig. 10** The drawing of photoelectric effect

### 2.3.4 Photoluminescence (PL) Spectrum

Photoluminescence is an important technique for measuring the purity and crystalline quality of semiconductors such as GaAs and InP, especially in the electrical structure. PL is a process in which a substrate absorbs photons (electromagnetic radiation) and then re-radiated photons. Quantum mechanically, this can be described as an excitation to a higher energy state and then a return to a lower energy accompanied by the emission of a photon corresponding to various recombination process in figure 11. During this process, there are six different kinds of recombination structure with emitting photons: free carrier recombination, free exciton recombination, bound exciton recombination, shallow level and Eigen inter-band carrier recombination, acceptor-donor recombination, and SHR recombination, which were related to the electronic structure, such as binding energy, exciton level, donor level and so on. Therefore, the PL process contains rich information of material structure and components in the material.



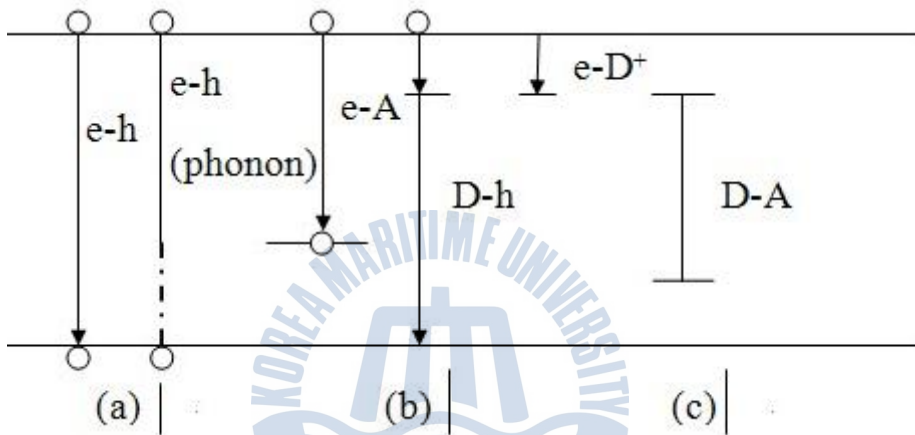


**Fig. 11** Various recombination processes in semiconductor (a) inter-band transition, (b) band-impurity center radiation recombination, (c) donor-acceptor radiation recombination

## Chapter 3. In doped ZnO nanorod

### 3.1 Experimental detail

In our research, we prepared indium doping ZnO nanorod by hydrothermal method using mixed solution of zinc nitrate hydrate, HMT, and indium acetate hydrate in different indium concentration on silicon substrate as shown table 2. Prior to hydrothermally method, approximately 100nm ZnO buffer layer was deposited on the silicon substrate by RF sputter. The morphological and photoluminescence properties were observed by field-emission scanning electron microscopy (FESEM), X-ray diffraction (XRD), and photoluminescence (PL) spectra. In addition, the chemical composition of In-doped ZnO nanorod was confirmed by X-ray Photoelectron Spectroscopy (XPS). Experimental results revealed the relationship of the morphology and indium concentration of ZnO nanorod.

**Table 2** The detail growth condition of un-doped ZnO and In doped ZnO with various indium concentration

Substrate		Si
Seed layer (thickness)		ZnO (100nm)
Temperature		95°C
Growth time		1 hour
Zinc concentration		0.025M
HMT concentration		0.025M
Doping condition	Doping material	Indium acetate hydrate
	In concentration	0, 5, 10, 25, and 50 wt.%

## 3.2 Results and discussions

### 3.2.1 Characterization of In-doped ZnO nanorod

Fig.12 shows the EDAX value of In-doped ZnO nanorods with various indium source concentrations. With increasing the indium source, the EDAX value of In-doped ZnO nanorod has an increase slightly, which indicates that the indium is introduced into the ZnO nanorod successfully although the value of EDAX is very low.

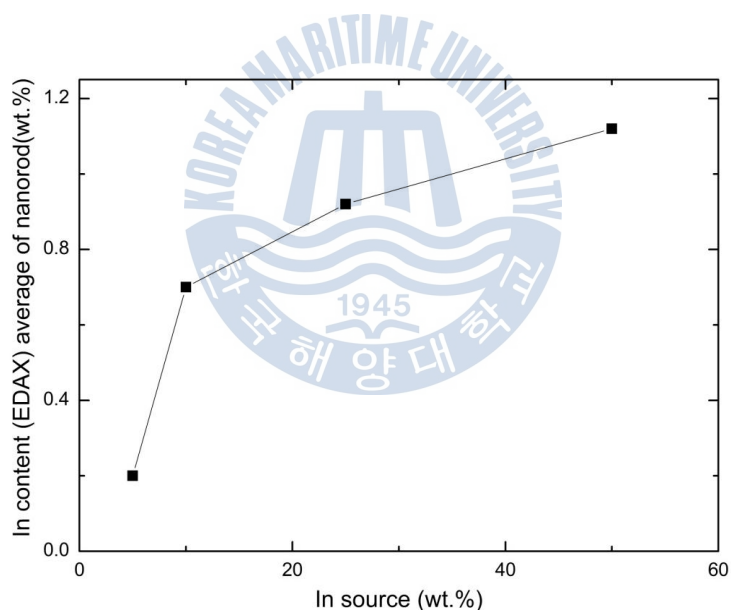


**Fig. 12** The In content (EDAX) value of In-doped ZnO nanorod with different In source varied from 5 to 50 wt.%

Fig.13 shows the XRD patterns of indium-doped ZnO nanorods on silicon substrate with various molar ratios of indium source. The diffraction intensity (vertical axis in the figure) is expressed in the logarithmic scale to allow the assessment of other secondary phases. The  $\theta$ - $2\theta$  XRD patterns of In-doped ZnO nanorod indicate that ZnO nanorods with preferred c-axis and indium compounds coexist. The detected XRD peaks are characteristic of well aligned ZnO with hexagonal wurtzite type crystalline structure. The pure ZnO nanorods show preferred growth orientation in the [0001] direction along the c-axis, in accordance with (002) peak of wurtzite structure with a similar result [9]. Once introduced into indium, the c-axis texturing was still mainly observed with In doped ZnO nanorods, together with one peak related to  $\text{In}_2\text{O}_3(\text{ZnO})_x$  coexists. However, the In-doped ZnO nanorods with 5 wt.% indium source show several kind of peaks such as (100), (101), (102), (110) as well as (002) peaks. With increase indium source, the (002) peak have a slight blue shift from  $34.45^\circ$  to  $34.41^\circ$  results from the bigger radius of indium compared to zinc, which suggests that the doping indium replace zinc sites of the ZnO lattice on some extent. The  $\text{In}_2\text{O}_3(\text{ZnO})_x$  peak appears and its intensity increase with the increase of indium source up to 25 wt.% and it has comparable intensity with (002) peak when indium source reached to 25 wt.%. The (002) peak decrease when the  $\text{In}_2\text{O}_3(\text{ZnO})_x$  peak increase. These results clearly indicate that the progressive incorporation of indium into the ZnO has different influence on the In-doped ZnO nanorod under various indium sources in consist with SEM images.



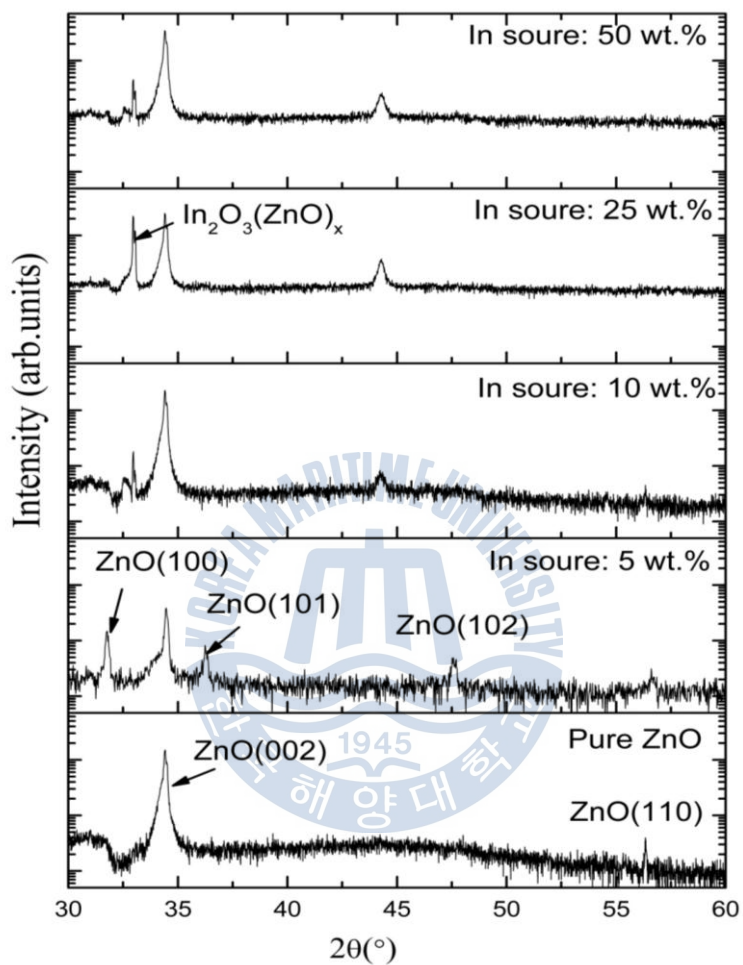


**Fig. 13** The XRD patterns of In-doped nanorod with various In source

Fig.14 shows the SEM images including cross section images of undoped ZnO nanorod and In-doped ZnO nanorod with different indium source varying from 5 to 50 wt.%, respectively. In planar view, the pure ZnO nanorod and In-doped ZnO nanorods have hexagonal shapes. From cross sectional images, most of the nanorods are vertical except the In-doped ZnO nanorod with 5 wt.% indium source with tilted direction in accordance with previous XRD results. Obviously, the In-doped ZnO nanorods are uniform with similar length compared to irregularity pure ZnO nanorod. It is well known that the nanorod size is decided by the number of the nucleation sites and the growth rate of crystal via hydrothermal method, which is related to the nanorod density and length of nanorod, respectively. As we could see, when the indium source was lower than 25 wt.%, the density of nanorod have a decrease as a whole and the length of In-doped ZnO nanorod increase with increasing indium source, which results of the increase of the nanorod's diameter size ( as shown in fig. 15). Here, we note that the diameter of In-doped ZnO with 5 wt.% indium source decrease to 0.05  $\mu\text{m}$  because of the increase of the nanorod density. On contrary, the length decrease when the indium source is 50 wt.%, which suggests that the growth rate become slower compared to other In-doped ZnO nanorods. Besides that, the density have a slightly increase. Thus, the diameter size of nanorod has an increase as a result of the slower growth rate and the larger nanorod density.

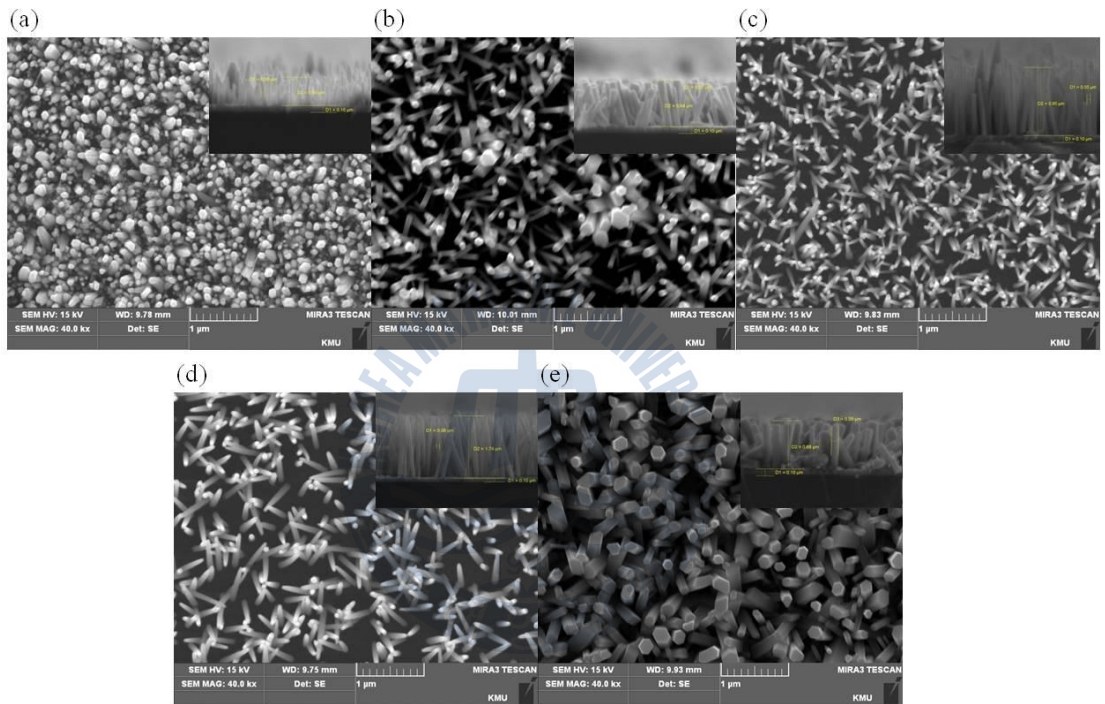


**Fig. 14** SEM images of In-doped ZnO nanorod: (a) pure ZnO nanorod, (b) indium source: 5 wt.%, (c) indium source: 10 wt.%, (d) indium source: 25 wt.%, (e) indium source: 50 wt.%.

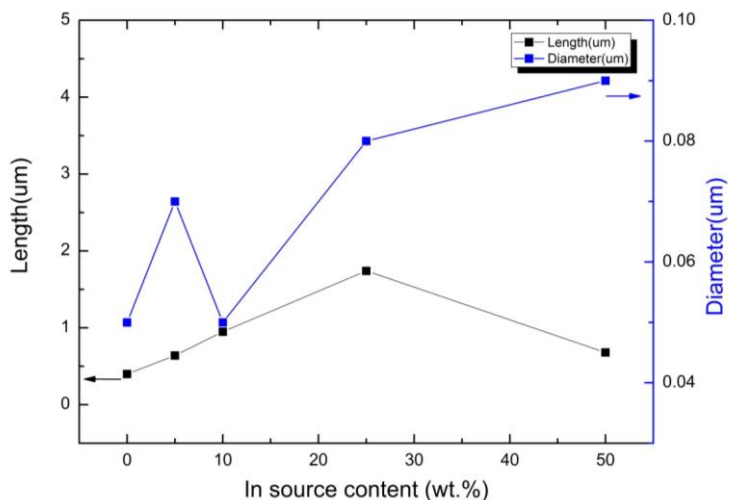


**Fig. 15** Diameters and length of pure ZnO and In-doped ZnO nanorods with different In source varied from 5 to 50 wt.%

Based on those results, the In dopant can improve the morphologies and the structural properties of In-doped ZnO nanorod. Hydrothermal growth of ZnO crystals in the presence of In ions was first reported in 1960s [10, 11]. Demianets et al. also reported morphological changes of ZnO crystal caused by  $\text{In}^{3+}$  in the solution [12]. But the growth mechanism of ZnO in the presence of indium is not yet well understood. Here, in order to explain these results, we supposed that the crystal growth is related to the the number of the nucleation sits and the growth rate of crystal via hydrothermal method as before.

Here, we supposed that, as the indium source concentration is under 25 wt.%, the number of the nucleation sites play the dominant role of the growth process of In-doped ZnO nanorods, which could be suspected form the XRD and the SEM results. The  $\text{ZnO}(\text{In}_2\text{O}_3)_x$  peak intensity increase with the indium source, which indicates that indium ions competes with zinc ions to form the growth units in the reaction solution. The decrease in the growth units will cause the reduction of the ZnO nuclei, which will let the In-doped ZnO nanorods grow free in c-axis. Therefore, the density of nanorod decrease

and the growth rate increase. Especially, the In-doped ZnO nanorod with 25 wt.% indium source exhibits the smallest density and longest length.

Contrarily, once the indium source concentration up to 50 wt.%, the growth rate of crystal is predominant rather than the density of the nucleation sites. The reduction of the  $\text{ZnO}(\text{In}_2\text{O}_3)_x$  peak intensity indicates that the density of In-doped ZnO nanorod is a little larger than In-doped ZnO nanorod with 25 wt.% indium source, although it is still smaller than pure ZnO nanorod. It was well known that the indium ions could block the crystal growth along c-axis when the indium concentration reached a certain value because it is easily absorbed into the top face of In-doped ZnO nanorod, (0001) face [13]. Therefore, the growth rate becomes slower than other In-doped ZnO nanorods. As a result, the diameter size of In-doped ZnO nanorod with 50 wt.% indium source have an increase and the its length have a decrease, but still larger than pure ZnO nanorod.

To obtain more information of the influence on the electric structure of ZnO by indium introduction and make sure the bonding states of ZnO:In nanorods, we did an investigation on the XPS spectrum of the pure ZnO and indium doped ZnO nanorods with 10 wt.% and 25 wt.%, respectively. Figure 16 (a) shows the full-range XPS spectrum using the photon energy 280eV. The XPS data only show Zn, O, and In peaks, which means that the indium is successfully absorbed into the ZnO nanorods. From that, we firstly defined that the In content of indium-doped ZnO nanorods with 10 wt.% and 25 wt.% were 0.4 at.% and 4.6 at.%, respectively.

The finely scanned Zn  $2p^{3/2}$  peak is shown in figure 16 (b). The Zn  $2p^{3/2}$  peak of undoped ZnO located at 1023 eV, larger than the characteristic value of Zn as metal, which suggests that Zn exists as combined form. As increasing the In content, the peak shifts towards to the lower energy different from other reports. It can be explained by the change of chemical surrounding of the  $\text{Zn}^{2+}$  ions. Atomic concentration of zinc and

oxygen was determined in table 3 and Zn/O ratio in the samples was equal to 1.128, 1.165, and 0.967 for pure ZnO, ZnO with 10 wt.%, and 25 wt.%, respectively.

The indium 3d peaks appear as in both elemental (453 eV) and in  $\text{In}(\text{OH})_3$  (445 eV) form, which verify the presence of indium ions on the surface of the doped particles (Fig. 16 (c)). It could be assumed that the indium might replace zinc sites as a substitutional donor or acts as interstitial impurity in the combined formation of In-O bonding. In/Zn ratio was calculated for the sample ZnO with 10 wt.% and ZnO with 25 wt.% and it was equal to 0.007 and 0.098.

The highly resolution of O 1s spectrum of the samples can be fitted into three peaks (Fig 16 (d)). The peak located at 530.6 eV belongs to the Zn-O bonding in ZnO, peaks located around 532.0 eV and 533.3 eV can be ascribed to the Zn-OH bonding related to the oxygen vacancy and to the presence of C=O bonding originated from the surface absorbed histidine molecules, respectively. As we could see, both of the areal ratio of peak (530.6 eV) and peak (532.0 eV) shown a slightly change (Table 4) which indicate that the indium doesn't replace zinc sites in large amount as a substitutional or occupy the oxygen vacancies but an interstitial impurity mostly.

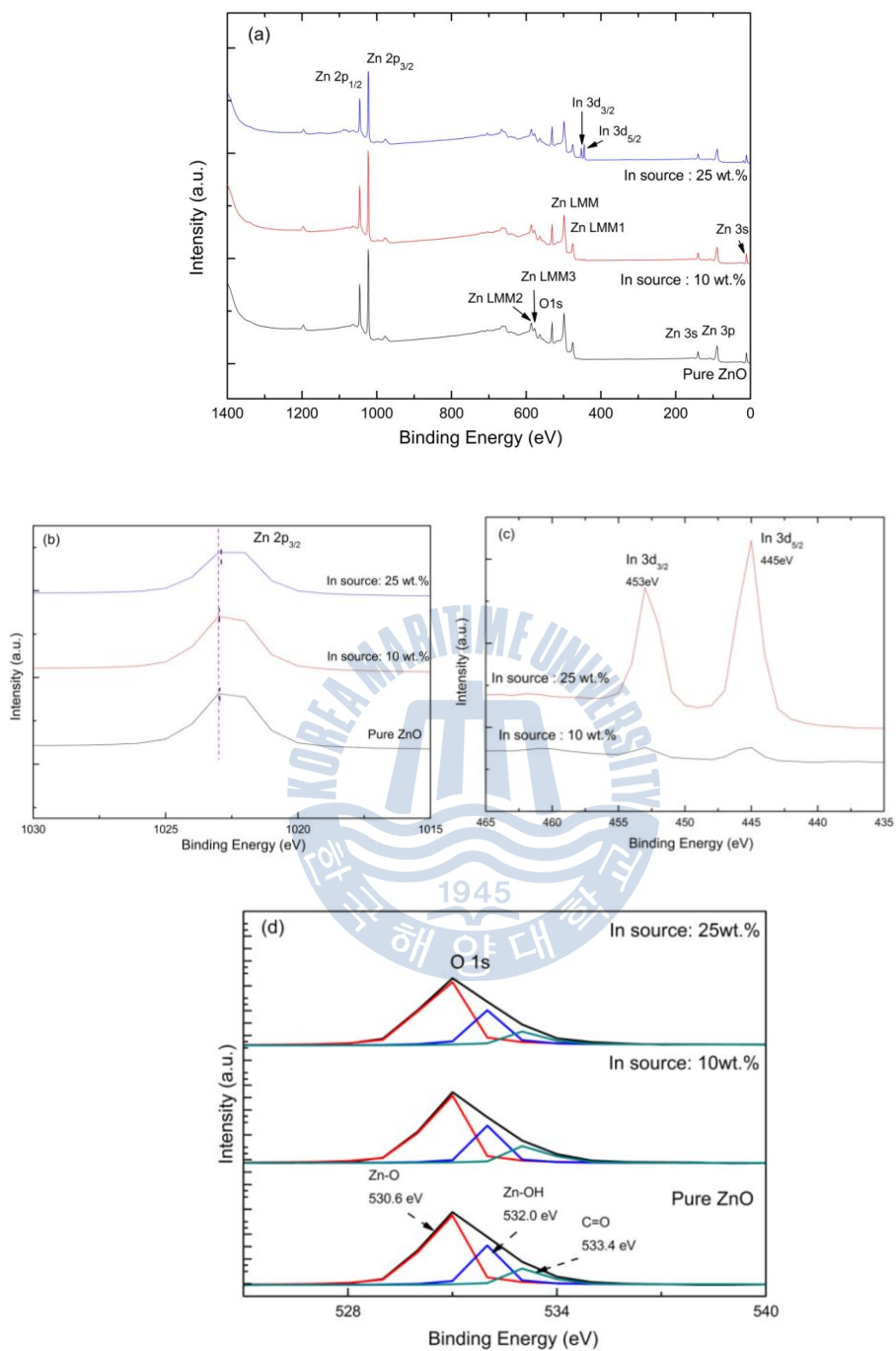


**Fig. 16** XPS spectrum: (a) full range, (b) Zn 2p<sub>3/2</sub>, (c) In 3d<sub>5/2</sub>, and (d) O 1s.

**Table 3** Atomic concentration of undoped ZnO and indium doped ZnO nanorods

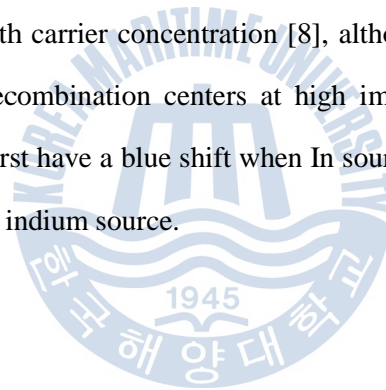
	Pure ZnO	In source: 10wt.%	In source: 25wt.%
Zn/O	1.128	1.165	0.967
In/Zn	-	0.007	0.098

**Table 4** The area ratio of different peak fitted into O 1s peak of different samples

	Pure ZnO	In source: 10 wt.%	In source: 25 wt.%
The area ratio of peak (Zn-O)	0.674	0.672	0.698
The area ratio of peak (Zn-OH)	18.512	16.574	19.676



To get better applications of opt-electrical devices, the photoluminescence properties of undoped ZnO and In-doped ZnO nanorod are measured at room temperature as fig. 17. The PL spectra show one sharp peak in the UV region, strong emission centered near 380nm. The dominant peak centers of undoped ZnO and In-doped ZnO nanorod with 5, 10, 25, and 50 wt.% are at 380.3, 380.0, 378.8, 381.2 and 380.9 nm, with dominant peak full-width at half-maximum (FWHM) values of 15.76, 15.56, 13.48, 12.39 and 15.61 nm, respectively. When In source under 25 wt.%, the UV band emission intensity increase with increasing of In source, together with the narrowing of FWHM value. On contrary, the UV band emission intensity decrease and the FWHM value increase dramatically as In source up to 50 wt.%. Various ZnO films doped with group-III atoms show an increase of UV band intensity along with carrier concentration [8], although it reduces owing to the increase of non-radiative recombination centers at high impurity concentration region. Besides that, the UV band first have a blue shift when In source was 10 wt.%, then have a red shift continuing increase indium source.



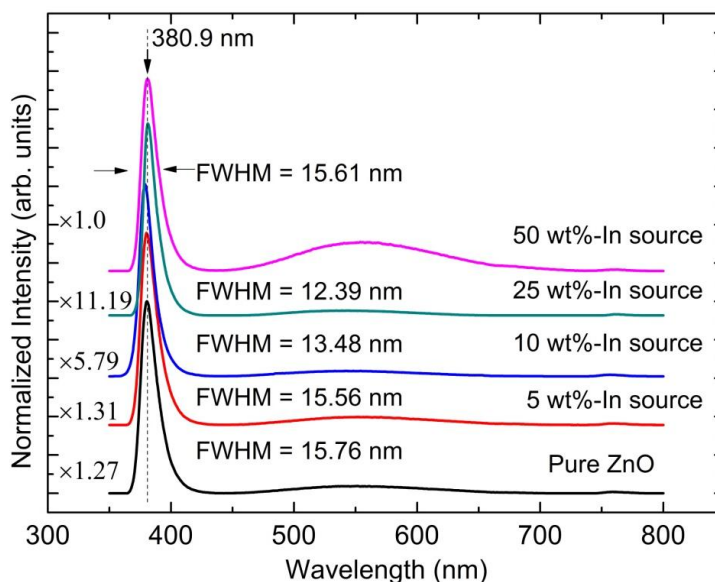


**Fig. 17** RT-PL patterns of pure ZnO and In-doped ZnO nanorod with different In source varied from 5 to 50 wt.%

The variation of PL intensity and peak position of In-doped ZnO nanorod could be summarized as follows; in low indium source concentration, the UV band intensity increases along with the carrier concentration after indium doping. However, when the indium concentration reached a certain amount, the UV band intensity begins to decrease due to the non-radiative recombination centers. The blue shift of the UV band could attribute to the shift of the optical band gap in these nanorods according to Burstein-Moss shift [14]. Once the indium concentration is as high as Mott density, red-shift of peak position will be accompanied due to the Mott shift.

Here, we note that when indium source was 50 wt.%, a weak visible emission band is observed as a deep level related to the oxygen vacancies [15]. What's more, the  $I_{uv}/I_{vis}$  is calculated for ZnO and In-doped ZnO nanorod in fig. 18. The ratio firstly increase as the indium source up to 25 wt.%, and then abruptly decrease when indium source reach 50 wt.%. We ascribe the decrease of the ratio and the appearance of deep level of In-doped

ZnO nanorod with 50 wt.% indium source to the weak exciton Coulomb interaction effect [16]. They explained that In acts as scattering center of exciton and generates the screened Coulomb potential field, which makes excitons ionized owing to losing Coulomb interaction. In conclusion, proper indium source doping could improve the optical properties of In-doped ZnO nanorod.

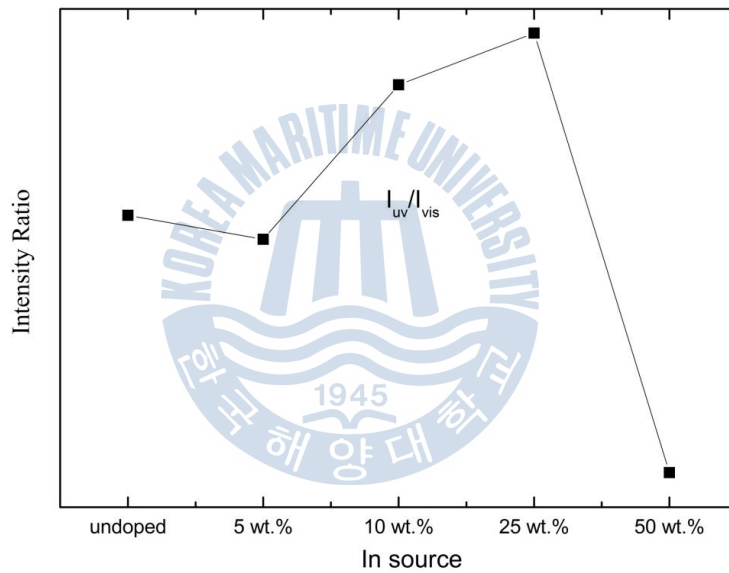
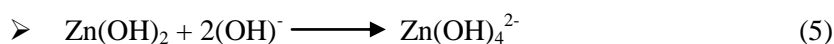
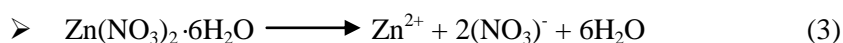
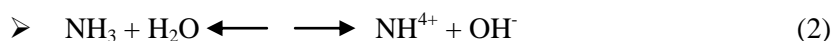


**Fig. 18** The intensity ratio of UV emission to visible emission of pure ZnO and In-doped ZnO nanorods

### 3.2.2 The growth mechanism of ZnO affected by indium impurity

Prior to considering the growth solution, we have proposed the chemical reaction of the hydrothermal method as before.



As we know, the interface of (0001) is occupied by relatively small zinc atoms with a positive charge, whereas (000-1) is terminated by oxygen atoms and has a negative charge. On the other hand, all six faces of {10-10} are all electrically neutral due to the same amount of zinc and oxygen atoms. We have assumed that the crystal growth is related with the incorporation of growth units onto the growth interface [18-20]. The incorporation rates of the growth units are different results from different interface structures and properties of the growth solution. As one of simplest growth units,  $\text{Zn}(\text{OH})_4^{2-}$  is negative charged complexes, an anionic coordination tetrahedron (see Eq.6). Since this anionic coordination growth units are easily incorporated into the positively charged (0001) zinc face, the ZnO nanorod naturally crystallizes in hexagonal structure.

When  $\text{In}^{3+}$  is present in the solution,  $\text{In}(\text{H}_2\text{O})_2(\text{OH})_4^+$  would produce octahedral

growth units (see Eq.7), which is easily incorporated into the zinc face. At the same time,  $\text{In}^{3+}$  ions could dissociated from  $\text{In}(\text{H}_2\text{O})_2(\text{OH})^{4+}$  (see Eq.8 ), which is easily incorporated into the oxygen face.

When small amount of indium was introduced into the solution,  $\text{In}^{3+}$  ions may be more likely species than  $\text{In}(\text{H}_2\text{O})_2(\text{OH})^{4+}$  in the solution. These ions tend to incorporate into the oxygen face, thus, ZnO crystals can still grow along c-axis. However, the crystal quality is reduced in these cases in accordance with the XRD results as before. On the other hand, the  $\text{OH}^-$  concentration decreases when the In content increase up to 25 wt.% ( the doping In content is small according to EDAX value lower than 1 wt.%) as a result of the competition of  $\text{In}^{3+}$  ion and Zn ion. So, the density of growth units ( $\text{Zn}(\text{OH})_4^{2-}$ ) have a slight decrease. Consequently, the diameter of In-doped ZnO nanorod increase as a function of the decrease of growth units.

Once the In content reached 50 wt.% (the doping In content is over 1 wt.%), the diameter of In-doped ZnO nanorod increase because of the block growth of zinc face. In contrast with In content under 1 wt.%, the octahedral growth units ( $\text{In}(\text{H}_2\text{O})_2(\text{OH})^{4+}$ ) is more than  $\text{In}^{3+}$  ions, which tend to incorporate into zinc face. So  $\text{In}^{3+}$  replaces zinc sites on some extent corresponding to the increase of (002) peak of In-doped ZnO nanorod. The octahedral growth units could protect the ZnO growth along c-axis, but permits the m-plane growth. What's more, the density of growth units has an increase following the increase in the  $\text{OH}^-$  concentration. Compared to the In-doped ZnO nanorod with In content under 1 wt.%, the In-doped ZnO nanorod with In content over 1 wt.% is uniform.

Finally, the experimental results revealed that the nanorod size could be changed tuning the indium concentration during nanorod growth.

## Chapter 4. In-doped ZnO nanostructure

### 4.1 Experimental detail

Compared to chapter 3, in this work, the doping material has been replaced into  $\text{In}_2\text{Cl}_3$  to get a deeper understanding of the growth mechanism of In-doped ZnO nanorod. The experimental conditions were described at detail in Tabel 5.

**Table 5** The detail growth condition of un-doped ZnO and In doped ZnO with various indium concentration

Substrate		Si
Seed layer (thickness)		ZnO (50nm)
Temperature		95°C
Growth time		1 hour
Zinc concentration		0.025M
HMT concentration		0.025M
Doping condition	Doping material	$\text{In}_2\text{Cl}_3$
	In concentration	10

## 4.2 Results and discussions

Obviously,  $\text{In}_2\text{Cl}_3$  is easily dissolved into the chemical solution which consists of zinc nitrate hydrate and HMT as a dopant material compared with the indium acetate hydrate. As shown in figure 19, the In-doped ZnO nanorod with bigger size were detected coexists with nominal size In-doped ZnO nanorod. Under this condition, we assumed that the  $\text{In}(\text{H}_2\text{O})_2(\text{OH})_4^-$  complex is more likely species than  $\text{Zn}(\text{OH})_4^{2-}$ . As a result, the growth of In-doped ZnO nanorod was blocked at some extent and the bigger size In-doped ZnO nanorod was immediately appeared due to the high concentration of  $\text{In}(\text{H}_2\text{O})_2(\text{OH})_4^-$ . On the other hand, the high concentration of  $\text{In}(\text{H}_2\text{O})_2(\text{OH})_4^-$  in the reaction solution may cause a deterioration at the seeded growth for In-doped ZnO nanorod.

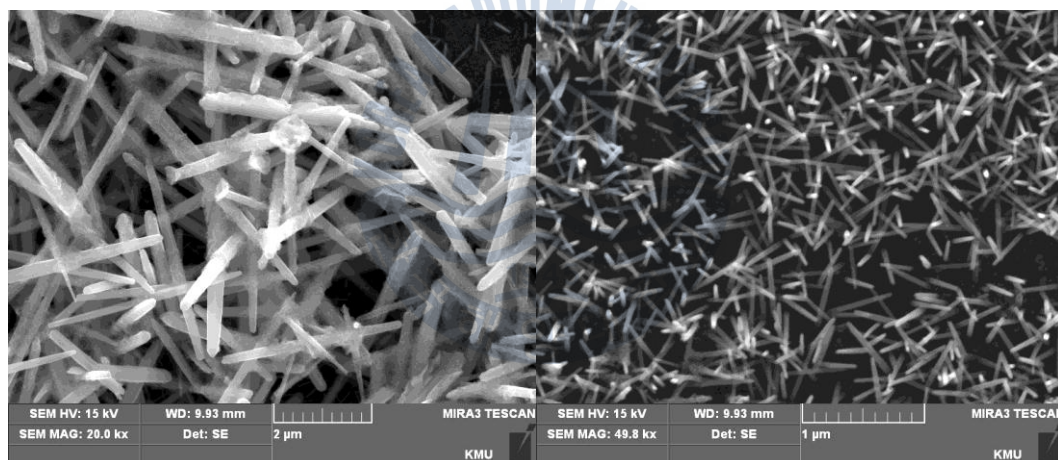


**Fig. 19** SEM images of In-doped ZnO nanorod with In content at 10 wt.%

## Chapter 5. Conclusion

In this work, we did research on the morphological and optical properties of ZnO nanorod with various In dopants and also the growth characteristics of ZnO nanostructure under hydrothermal conditions as influenced by indium ions have been studied.

The In-doped ZnO nanorod was successfully grown by hydrothermal method under different indium source concentration. With increasing indium source concentration, the progressive incorporation of In into the compounds first caused a deterioration and then improvement of In-doped ZnO nanorod. The growth mechanism varied by different In content. When the indium source was under 25 wt.%, the diameter size and length of In-doped ZnO nanorod have an increase in whole due to the predominant role of the density of nucleation site. The increase of  $I_{uv}/I_{vis}$  indicates that the indium doping cause an improvement of the optical properties of In-doped ZnO nanorod. On contrast, the In-doped ZnO nanorod with 50 wt.% indium source have a larger diameter and shorter length results from the slower growth rate. At the same time, the  $I_{uv}/I_{vis}$  decrease dramatically which suggests that over indium source could have a deterioration of its optical properties.

Besides that, In-doped ZnO nanostructures were grown by different indium dopant material under different In content. The  $InCl_3$  were easily dissolved into the chemical reaction solution used for grown ZnO compared to zinc acetate hydrate. As a result, the In-doped ZnO nanorod with big size were formed due to the high growth unit of  $In(H_2O)_2(OH)^+$  in the chemical solution. on the other hand, the nominal size In-doped ZnO nanorod were still detected with poor crystalline quality because of the decrease of growth units of  $Zn(OH)_4^{2-}$ .

In conclusion, the morphological, structural, optical properties of In-doped ZnO



nanorod could be changed tuning the changing of In content via different growth mechanism under different In content. What's more, the growth mechanism also could be changed by different indium dopant materials due to the different ability of dissolve into the reaction solution.



## References

- [1] Y. H. Ni, X. W. Wei, J. M. H and Y. Y, Materials Science and Engineering B, 121, 42 (2005)
- [2] Chu et al., Nanoscale Res Lett. 6:38 (2011)
- [3] Ridhuan N S, Abdul PazaK K, Lockman Z, Abdul Aziz A, PloS ONE 7(11):e50405 (2012)
- [4] A. B. Djurisi, Y. H. Leung, K. H. Tam, L. Ding and W. K. Ge et al., Appl. Phys. Lett. 88, 103107 (2006)
- [5] U. Rau and M. Schmidt, Thin Solid Films. 387, 141 (2001)
- [6] Gorla, C.R et al., J. Appl. Phys. **85**, 2595 (1999)
- [7] M. -H. Zhao, Z. -L. Wang and S. X. Mao, Nano Lett. 4. 587 (2004)
- [8] R. Ferro, J. A. Rodrihuez, P. Bertrand, 2008. Thin Solid Films 516 2225 (2008)
- [9] Junjie Qi, Yue Zhang, Yunhua Huang, Qingliang Liao and Juan Liu, Appl. Phys. Lett. 89. 252115 (2006)
- [10] A. Escobedo-Morales and U. PaI, Appl. Phys. Lett. 93. 193120 (2008)
- [11] Jiansheng Jie, Guanzhong Wang, Xinhai Han, Qingxuan Yu, Yuan Liao, Gongpu Li, and J. G.Hou, Chemical physics letter. 387. 466 (2004)
- [12] C. Klingshirn, Chem. Phys. Chem. 8. 782 (2007)
- [13] T. Fang and S. Kang, Current Applied Physics. 10. 1076 (2010)
- [14] Buguo Wang, M. J. Callahan, Chuanchuan Xu, L. O. Bouthillette, N. C. Giles and D. F. Bliss, Journal of Crystal Growth. 304. 73 (2007)

- [15] E. D. Kolb, R. A. Laudise and J. Am, Ceram. Soc. 49 302 (1966)
- [16] R. A. Laudise, E. D. Kolb, A. J. Caporaso and J. Am, Ceram. Soc. 47 9 (1964)
- [17] L. N. Demianets, L. V. Kostomarov, I. P. Kuzmiza and S. V. Pushko, Crystallogr. Rep. 47 S86 (2002)
- [18] B. Wang, E. W. Shi, and W. Z. Zhong, Crystal Res. Technol. 32 659 (1997)
- [19] B. Wang, E. W. Shi and W. Z. Zhong, Chinese Sci. Bull. 42 1041 (1997)
- [20] B. G. Wang, E. W. Shi and W. Z. Zhong, Crystal Res. Technol. 35(3) 279 (2000)

